Consequences of optical pumping and interference for excitation spectra in a coherently driven molecular ladder system

N. N. Bezuglov,[1,2] R. Garcia-Fernandez,[3] A. Ekers,[2] K. Miculis,[2] L. P. Yatsenko,[4] and K. Bergmann[5]
[1]*Faculty of Physics, St. Petersburg State University, 198904 St. Petersburg, Russia*
[2]*Laser Centre, University of Latvia, LV-1002 Riga, Latvia*
[3]*Department of Physics, University of Mainz, D-55128 Mainz, Germany*
[4]*Institute of Physics, Ukrainian Academy of Sciences, 03650 Kiev, Ukraine*
[5]*Department of Physics, University of Kaiserslautern, D-67663 Kaiserslautern, Germany*
(Received 5 August 2008; published 5 November 2008)

This paper presents observations and an interpretation of laser-induced excitation and fluorescence in a ladder *g-e-f* of three molecular levels [$X\,^1\Sigma_g^+(v''=0,J''=7)$, $A\,^1\Sigma_u^+(v'=10,J'=8)$, and $5\,^1\Sigma_g^+(v=10,J=9)$, respectively] observed in a supersonic molecular beam of Na_2. The *g-e* coupling, by cw laser *P*, is strong. A weak cw laser *S* couples levels *e* and *f*. The basic observations are of level-*f* fluorescence as a function of the detuning of the *S* laser from resonance. The signal profile does not appear as the typical Autler-Townes doublet, but as a spectral structure, whose position, width, and shape depend upon several laser parameters. We interpret these results using a simple model of three nondegenerate quantum states coherently excited while undergoing population loss to states outside the three-level system. We invoke the mechanism of optical pumping and evolution along adiabatic states, together with Landau-Zener transition probabilities. We also present results from numerical studies, which include all quantum states, all radiative couplings, coherent and incoherent, as well as convolutions with the relevant distribution functions (velocities and Zeeman sublevels). Although no adjustable parameters are involved, excellent agreement with the experiment is found. Since successive avoided crossings of adiabatic eigenvalues occur, interference effects may be relevant. Such effects are not expected to be visible in the present experiment, for reasons that are discussed. However, we discuss conditions which would allow resolving the interference structure experimentally. We also suggest possible interesting applications of the interference to rapidly switch off Rydberg state population or to control its spatial distribution.

DOI: 10.1103/PhysRevA.78.053804 PACS number(s): 42.50.Hz, 33.80.−b, 33.40.+f, 33.70.Jg

I. INTRODUCTION

A. Background and motivation

The Autler-Townes effect (AT) has been studied in detail in atoms [1,2], but less extensively in molecules [3,4]. When transitions between two levels are driven by strong coherent radiation fields and the population in one level is probed by a relatively weak field, the Autler-Townes splitting of spectral lines typically appears as a doublet structure in the excitation spectrum [5].

In molecules, any radiatively coupled three-level system is an open one due to many possible rovibrational transitions. Their population will be lost by decay to levels other than those coupled by the laser fields. Therefore a typical scheme for demonstrating AT would use a strong field which couples two unpopulated excited levels, while the fluorescence induced by a weak probe field which drives a small fraction of the population into the excited states is observed [3,4].

In our study we consider an open three-level ladder system *g-e-f* in Na_2 molecules (see Fig. 1). A strong laser field couples a populated electronic ground state level *g* with the level *e*, which is the lower one of two excited levels *e* and *f*. The frequency of a weak laser *S* is tuned across the resonance frequency of the *e-f* transition. In such an arrangement, no AT doublets appear in the *S*-laser induced excitation spectrum. Instead, peculiar spectral profiles are observed. Depending on the frequency of the strong laser, either one narrow structure is observed when the laser frequency is on resonance with the *g-e* transition, or a broad spectral profile with its center shifted in frequency is recorded when the strong laser is tuned off resonance. Most importantly, no doublet structure is observed. The processes leading to such spectral profiles are nontrivial. In what follows we shall explain the physics underlying these processes, using a simplified model based on adiabatic states. We also provide an accurate numerical analysis based on the solution of density matrix equations of motion.

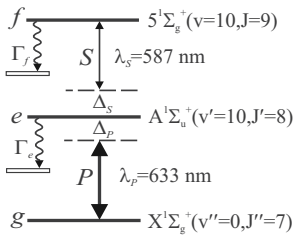

FIG. 1. Three-level ladder linkage in Na_2. Levels *g* and *e* are coupled by a strong *P* laser, nominally of wavelength 633 nm and detuned from resonance by Δ_P. A weak *S* laser, nominally 587 nm and detuned from the *e-f* resonance by Δ_S, brings population into level *f*. Spontaneous emission, observed as spectrally unresolved fluorescence, occurs from levels *e* and *f*, as indicated by wiggling arrow-headed lines. Our observations of excitation spectra consist of measuring the fluorescence from level *f* as a function of the probe detuning Δ_S.

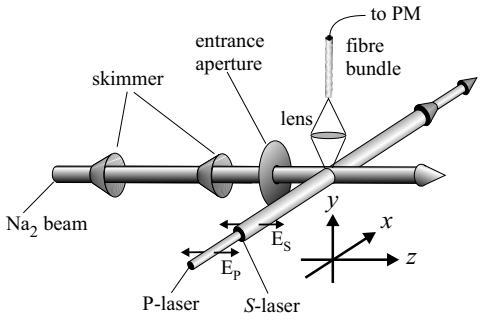

FIG. 2. Geometry of the experiment. The collinear laser beams define the x direction. The molecular beam axis and linear polarization directions of laser fields are parallel to the z axis, which serves as the quantization axis for the molecular orientation.

B. Experiment

In the experiment we measured laser-induced excitation spectra for a three-level molecular system in Na_2 molecules in a collimated molecular beam. The sodium dimers are excited and probed as they fly across two focused collinear laser beams (termed S and P). Figure 2 defines the geometry of the experiment. Both lasers are linearly polarized in the direction of the molecular beam axis, which serves as the z axis (and as the quantization axis for molecular orientation).

The laser-induced excitation is a two-step process, involving the rovibrational levels shown schematically in Fig. 1. The levels g, e, and f are, respectively, the ground level $X\ ^1\Sigma_g^+(v''=0,J''=7)$, an excited level $A\ ^1\Sigma_u^+(v'=10,J'=8)$, and a final level $5\ ^1\Sigma_g^+(v=10,J=9)$. The laser responsible for coupling the levels g and e is labeled P; the laser labeled S provides weak coupling of level e to level f. We record the fluorescence from level f as we vary the S-laser detuning Δ_S for fixed P-laser detuning Δ_P. The laser-induced fluorescence signal traces out a resonance feature that we refer to as a *spectral profile*. Our principal results deal with the spectral width and central frequency of this profile, as well as the shape of the profile. We discuss also how these parameters are affected by controllable laser characteristics. Our interpretation of these features invokes optical pumping as well as special features of coherent-excitation processes.

C. Model

The modeling of laser-induced excitation processes for molecules in a beam must account for appropriate ensemble averages over parameters which are not precisely controlled. In addition to the change of molecular level populations caused by spontaneous emission, the following characteristics must be considered:

(1) Doppler detuning. The distribution $f(v_\perp)$ of the velocity component $v_\perp$ perpendicular to the molecular beam axis (and parallel to the direction of laser propagation) causes a distribution of Doppler shifts and hence a distribution of laser detunings.

(2) Variable transit times. As a molecule moves through a laser beam it experiences a pulsed electric field—it is this field that induces the excitation. The distribution $f(v_\parallel)$ of the velocity component $v_\parallel$ parallel to the molecular beam axis around the mean velocity of the molecules in the beam causes a distribution of the duration of the interaction with the laser beams, and hence a distribution of excitation probabilities.

(3) Varying orientation. A molecule with an angular momentum J has $2J+1$ distinguishable orientations, each one characterized by a magnetic quantum number m_J. The interaction strength of the molecule with the radiation field depends upon the angle between the electric field vector and the molecular dipole moment, and hence there occur $2J+1$ distinct values of this interaction strength.

We introduce first a simplified three-state "average molecule" model, to provide an illustrative interpretation of our experimental results. We idealize the actual molecule as a system of three nondegenerate quantum states, labeled g, e, and f. Effects of thermal motion are initially neglected, as are orientation averages. We consider mean values for the interaction strengths, as parametrized by Rabi frequencies. The radiative lifetimes of the excited levels e and f are smaller than or comparable to the excitation times, as set by the transit time across the beam. Almost all of the decay processes from e and f proceed to levels outside our three-level manifold—this is an example of an "open" system. Therefore, for the purpose of illustration we treat spontaneous emission as a loss from states e and f. However, in the more detailed numerical model described in Sec. V, we consider all possible couplings between the magnetic sublevels of the levels g, e, and f, including the spontaneous decay from level f to level e and from level e to level g. We also include the appropriate convolution over the relevant distribution functions mentioned above.

Our model system involves strong coupling of the ground and the first excited state, well suited for using the concept of adiabatic states. The strongly coupled two-level system (g-e) is probed by weak coupling to the final fluorescing state f. The observed fluorescence signals are interpreted based on the variation of adiabatic eigenvalues as a function of the position within the laser beam (or as a function of time, since a given molecule travels at constant speed), as well as on their dependence on intensity (Rabi frequency) and detuning.

II. EXPERIMENTAL SETUP

The experimental setup used for the present work has been described in detail earlier [4]. The axis of a supersonic beam of Na_2 molecules crosses the coaxial P- and S-laser beams at right angles. The mean molecular flow velocity was $v_m=1340$ m/s. The longitudinal velocity distribution (contributing to Doppler detuning) had a full $1/e$ width $\Delta v_\parallel = 520$ m/s. Two skimmers and an entrance aperture at the excitation zone collimated the beam to a divergence angle of 0.85°. The corresponding residual transverse velocity spread was $\Delta v_\perp = 10$ m/s (full $1/e$ width).

The two laser beams, with wavelengths $\lambda_P=633$ nm and $\lambda_S=587$ nm and powers of 340 and 0.35 mW, respectively, were generated by coherent CR-699-21 cw ring dye lasers with a linewidth of 1 MHz. Both laser beams were linearly polarized, with the direction of polarization parallel to the molecular beam axis.

The beams were focused using a cylindrical lens such that the long axis of the focus was perpendicular to the molecular beam axis (the y direction). Along the molecular beam axis the spatial intensity profiles were Gaussian,

$$I_j(z) = I_j^{(0)} \exp(-\ln 2z^2/R_j^2), \quad j = P,S, \tag{1}$$

with waists $R_P=50$ μm and $R_S=150$ μm. The P-laser waist was substantially smaller than that of the S laser because the P laser was more tightly focused onto the axis of the molecular beam.

In the moving frame of a molecule this intensity distribution leads to a time varying Rabi frequency

$$\Omega_j(t) = \Omega_j \exp(-\ln 2t^2/2\tau_j^2), \quad j = P,S, \tag{2}$$

where $\tau_j=R_j/v_m$ and $\Omega=\mu\varepsilon/\hbar$; μ is the relevant transition dipole moment and ε is the amplitude of the electric field. The transit time of the molecules through the P-laser beam was $\tau_{tr}=2R_P/v_m \simeq 75$ ns. This is longer than the natural lifetime of the level e, $\tau_e=12.45$ ns [6] and level f, $\tau_f=35$ ns [7].

From the laser intensity used in the experiment and using the mean values for the transition dipole moments and measured values of peak intensity we determine the Rabi frequencies to be $\Omega_P/2\pi=339$ MHz and $\Omega_S/2\pi=3$ MHz. Thus Ω_S is about two orders of magnitude smaller than Ω_P. Furthermore, because of the less tight focusing of the S laser, Ω_S varies spatially little over the range where Ω_P is nonzero.

The fluorescence emitted from molecules in the excitation zone in the y direction (perpendicular to the plane defined by the axis of the molecular beam and the laser beams), was focused into a multicore fiber bundle, which was not polarization sensitive, and detected by a photomultiplier and a photon counter (see Fig. 2). A bandpass filter restricted the light which reaches the detector to the fluorescence from the upper level $5\ ^1\Sigma_g^+(v=10,J=9)$.

III. EXPERIMENTAL RESULTS

Figure 3 shows an example of excitation spectra (total fluorescence from the upper level f) as a function of the S-laser detuning Δ_S for various values of the P-laser detuning Δ_P. The circles are the experimental values and the lines are results of numerical calculations discussed in Sec. V.

The spectral profiles vary significantly with Δ_P. Unlike the results obtained for a similar three-level coupling scheme in Na atoms [8,9], which was used in the first demonstrations of the Autler-Townes effect in the optical domain, no doublet is observed. Instead, for resonance, $\Delta_P=0$, only one relatively narrow peak occurs, reaching a maximum when the S laser is at resonance, $\Delta_S=0$. With moderate Δ_P this spectral feature broadens, and its center shifts and narrows again with a further increase of Δ_P.

IV. QUALITATIVE ANALYSIS

A. Adiabatic states

The qualitative interpretation of the observations is based on the adiabatic states for the strongly coupled two-level

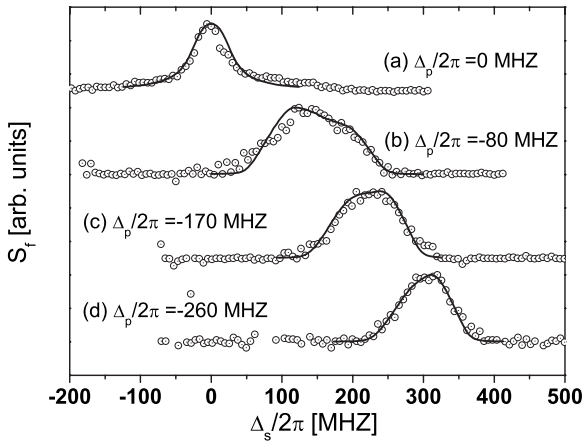

FIG. 3. Fluorescence signal S_f from the upper level f as a function of the S-laser detuning $\Delta_S/2\pi$ for various choices of the P-laser detuning $\Delta_P/2\pi$ (a) 0 MHz, (b) −80 MHZ (or $\Delta_P/\Omega_P=-0.21$), (c) −170 MHz (or $\Delta_P/\Omega_P=-0.45$), (d) −260 MHz (or $\Delta_P/\Omega_P=-0.69$). Circles represent the experimental results, and solid lines show the results of the numerical simulations described in Sec. V B. The spectra for positive detunings of Δ_P (not shown) are mirror reflections of the spectra for $\Delta_P<0$ with respect to $\Delta_S=0$.

system (a simplified model). Disregarding losses due to spontaneous emission, the Hamiltonian reads in the rotating wave approximation [10],

$$H = \hbar \begin{bmatrix} \Delta_P & \frac{1}{2}\Omega_P \\ \frac{1}{2}\Omega_P & 0 \end{bmatrix}. \tag{3}$$

It involves the detuning Δ_P, defined as $\Delta_P=\omega_P-(E_e-E_g)/\hbar$ and the Rabi frequency $\Omega_P=d_{ge}\mathcal{E}_P(t)/\hbar$, where $\mathcal{E}_P$ is the amplitude of the electric field for the P laser and d_{ge} is the z component of the transition-dipole moment of the transition g-e between the levels g and e.

The fluorescence signal S_f is proportional to the radiative decay rate Γ_f of level f and to the instantaneous population of that state. The contribution of a given group of molecules to S_f is time dependent because the molecules move with constant velocity v_m across the spatially varying field. Thus, the Rabi frequencies experienced by that group of molecules are time dependent. However, the measured signal S_f is neither time, nor space resolved. It is proportional to the population of state f integrated over time and space. We refer to the variation of the intensity of this fluorescence signal $S_f(\Delta_S)$ with the S-laser detuning Δ_S as the spectral shape.

It is well known from textbooks [10] that the eigenfunction and eigenvalues of Eq. (3) are

$$H\Phi_\pm = \hbar\varepsilon_\pm\Phi_\pm, \tag{4}$$

with

$$\varepsilon_\pm = \frac{1}{2}\left[\Delta_P \pm \sqrt{\Delta_P^2+\Omega_P^2}\right], \tag{5}$$

and

$$\Phi_- = \cos\,\theta_P \psi_e - \sin\,\theta_P \psi_g, \tag{6}$$

$$\Phi_+ = \sin\,\theta_P \psi_e + \cos\,\theta_P \psi_g. \tag{7}$$

Since these states are defined in a rotating frame, the implicit time dependence, at carrier frequency, is hidden. The mixing angle θ_P is defined through $\tan(2\theta_P)=\Omega_P/\Delta_P$ with the constraint $0 \leqslant \theta_P \leqslant \pi/2$. At vanishing intensity, i.e., $\Omega_P=0$, the adiabatic states relate to the original bare states. If $\Delta_P<0$ and $\Omega_P \to 0$, then $\tan(2\theta_P)$ approaches zero from the side of negative values and reaches it at $\theta_P=\pi/2$. With the eigenvalues from Eq. (5) we have

$$\Phi_- \to -\psi_g, \quad \varepsilon_- \to \Delta_P, \tag{8}$$

$$\Phi_+ \to \psi_e, \quad \varepsilon_+ \to 0. \tag{9}$$

If $\Delta_P>0$, then in the limit $\Omega_P \to 0$ the value of $\tan(2\theta_P)$ is zero at $\theta_P=0$, and we obtain the correlation

$$\Phi_- \to \psi_e, \quad \varepsilon_- \to 0, \tag{10}$$

$$\Phi_+ \to \psi_g, \quad \varepsilon_+ \to \Delta_P. \tag{11}$$

The population resides initially in state g. Thus prior to the interaction with the P laser the state vector coincides with the adiabatic state Φ_-, while the excited state relates to Φ_+ ($\Delta_P<0$). If the evolution is adiabatic, the state vector remains in state Φ_- as long as the S-laser intensity is zero.

The P-laser interaction transforms the state vector into a superposition of states g and e. Depending on the value of Ω_P and Δ_P, the contribution from state e may be as large as 50%. For a given Ω_P the contribution of state e to the state vector decreases with increasing Δ_P. It is only the population of this e component of the state vector that can be excited to state f by the S laser.

In the basis of states $\{\Phi_-, \Phi_+, \psi_f\}$, i.e., the coherent superposition of the strongly coupled states g and e, plus the state f, which is only weakly coupled to the former, the Hamiltonian reads in the adiabatic approximation

$$H' = \hbar \begin{bmatrix} \varepsilon_- & 0 & \frac{1}{2}\Omega_- \\ 0 & \varepsilon_+ & \frac{1}{2}\Omega_+ \\ \frac{1}{2}\Omega_- & \frac{1}{2}\Omega_+ & \varepsilon_f \end{bmatrix}, \tag{12}$$

where

$$\varepsilon_f \equiv -\Delta_S, \tag{13}$$

and $\Omega_\pm$ is the coupling strength between the adiabatic states $\Phi_\pm$ and state f. This Hamiltonian serves to identify the locations where resonances occur. The dynamics of the evolution, including decay, is treated numerically in Sec. V.

The contribution of the states g and e to the eigenstates $\Phi_\pm$ and the adiabatic eigenvalues $\varepsilon_\pm$ vary with the position of the molecule in the laser beam profile and hence with time in the reference frame of the moving molecule. Whenever two diagonal elements of the Hamiltonian are degenerate

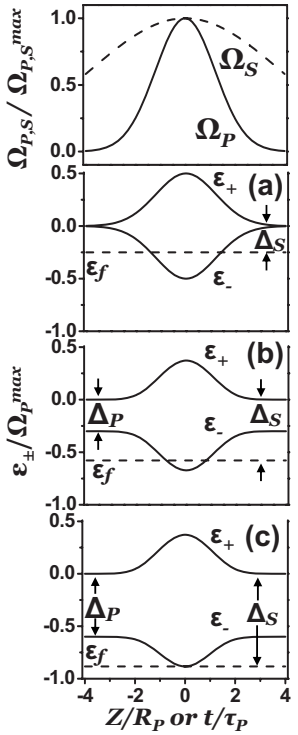

FIG. 4. Adiabatic eigenvalues ε_-, ε_+, and $\varepsilon_f=-\Delta_S$, in units of Ω_P^{max} versus $t/\tau=z/R_P$. (a) $\Delta_P=0$, $\Delta_S=-0.5\varepsilon_-^{min}$; (b) $\Delta_P=-0.3\Omega_P^{max}$, $\Delta_S=-0.75\varepsilon_-^{min}$; (c) $\Delta_P=-0.6\Omega_P^{max}$, $\Delta_S=-1.0\varepsilon_-^{min}$. At each crossing of the curves ε_- and f, population transfer occurs. There are two spatially located regions for such transitions: one for $t<0$ and the other for $t>0$.

(i.e., equal) [20], transitions between Φ_+ or Φ_- and f will occur. For a system described by the Hamiltonian (12) this will occur when $\varepsilon_f=\varepsilon_-$ or $\varepsilon_f=\varepsilon_+$; that is, when

$$\Delta_S = -\varepsilon_\pm. \tag{14}$$

B. Interpretation of the excitation spectra

Figure 4 presents a plot of the eigenvalues $\varepsilon_\pm$ along with ε_f, showing the variation with either position z or time t in the molecular reference frame for fixed Δ_S and three choices of the detuning Δ_P as follows:

(1) Resonant P field: $\Delta_P=0$.

(2) Moderate P field detuning: $|\Delta_P| \lesssim \Omega_P$.

(3) Large P field detuning: $|\Delta_P| > \Omega_P$.

For sufficiently small detuning Δ_P, the resonance condition (14) occurs at two spatially restricted regions: one for $z_1<0$ (or $t_1<0$), and the other for $z_2>0$ (or $t_2>0$). The maximum (minimum) of ε_+ (ε_-) is at $z=0$. Therefore, the state vector may evolve along two paths. At the crossing of ε_f and ε_- the population in Φ_- may remain in that level and thus follow the path ε_- or may be transferred to level f and then follow the path ε_f. At z_2 ε_- and ε_f cross again and the populations in Φ_- and f may again branch off along either ε_- or ε_f depending on the coupling strength. Since phase difference will be accumulated during the propagation along ε_- and ε_f, the asymptotic population in f will be affected by interferences.

Taking spontaneous emission into account is essential for the understanding of the spectral shape, i.e., the variation of the fluorescence intensity $S_f(\Delta_S)$ from level f as a function of Δ_S for a given Δ_P (see Fig. 3). The signal $S_f(\Delta_S)$ does not carry information about the spatial distribution of molecules in state f, because fluorescence is collected from all locations along the z axis within the laser beam profile. Nevertheless, we shall comment in Sec. VI on the spatial distribution of molecules in state f when discussing interference phenomena.

When the P laser is on resonance [Figs. 3(a) and 4(a)], one would expect a well-developed (symmetric) AT doublet. However, optical pumping prevents the appearance of an AT doublet. The population in the levels g and e is lost by optical pumping to other levels in the early wings of the laser beam profiles, since the spontaneous emission lifetime is much shorter than the transit time through the laser beam. There may be some broadening, but no splitting. The population is gone before the splitting is large enough to be seen.

When the P laser is off resonance [see Figs. 3(b), 3(c), and 4(b)], the rate of optical pumping is smaller. Furthermore, only one of the adiabatic states Φ_- or Φ_+ is populated. The other one, which would lead to the second AT peak shifted in frequency, is not populated and thus is not seen. Depending on the coupling strength Ω_S, a fraction of the population evolves along ψ_f, the other along Φ_- or Φ_+. The rate of optical pumping is no longer sufficiently large to deplete the population of the adiabatic state before the second crossing between ε_+ and ε_f at $z_2>0$ is reached. Therefore, excitation to level f is possible over a range of Δ_S, determined by Ω_P, and a broader spectral structure is observed. Furthermore, how much population will reside in state f after the second crossing of ε_- and ε_f depends on the phase difference accumulated during the two paths, which became accessible at the first crossing of ε_- and ε_f for $z_1<0$. Thus, the spectral profiles may show some additional structure [see Figs. 3(b) and 3(c)], and the discussion below.

When the detuning Δ_P of the P laser is large [see Figs. 3(d) and 4(c)], the coupling is weak and thus optical pumping is negligible. Furthermore, the Stark shift of level Φ_- is rather small and thus the spectral profile $S_f(\Delta_S)$ of the fluorescence is narrow, but with its center shifted by $\approx\Delta_P$ as compared to the profile for $\Delta_P=0$. Also, the phase difference between the two pathways is smaller and thus interference, if observable at all, will be less pronounced.

V. QUANTITATIVE ANALYSIS

So far we have considered a simplified molecular ladder level system. We now present the results of numerical calculations, which avoid any significant simplifications. In particular, the full set of magnetic sublevels m_J of the states g, e, and f are included. Even when the P and S lasers are linearly polarized, implying the selection rule $\Delta m_J=0$, the population of neighboring sublevels is affected by spontaneous emission. About 5% of the population returns from level e to level g via spontaneous emission. Spontaneous emission brings more than 30% of the population from level f back to level e. Therefore we model the excitation spectra using the density matrix equations of motion and account for all possible couplings.

A. Density-matrix equation of motion

The numerical calculations were done by solving the density-matrix equation

$$\frac{d\rho}{dt} = -\frac{i}{\hbar}[H,\rho] - \frac{1}{2}(\Gamma\rho + \rho\Gamma) + L\rho. \tag{15}$$

The density matrix $\rho(t)$ provides the time dependence of the populations of all magnetic sublevels of the g-e-f ladder system and all possible optical and Zeeman coherences for an ensemble of molecules flying across the laser beam. The Hamiltonian H includes all the couplings between Zeeman sublevels induced by P and S lasers. The matrix Γ gives the depletion rates of the magnetic sublevels due to the spontaneous emission to levels within and outside the g-e-f system. The matrix $L(\rho)$ gives the rates of population increase of magnetic sublevels due to the spontaneous transitions from other sublevels of the system. This matrix has a simple explicit form in the representation of polarization moments [11]. We solve Eq. (15) in the rotating wave approximation (RWA) [10,12] numerically, using the split propagation technique (SPT) [13,14].

B. Theoretical excitation spectra

The fluorescence signal S_f observed in the experiment is proportional to the time-integrated total population of level f.

$$S_f \sim \sum_{m_J} \int_{-\infty}^{\infty} dt \rho^f_{m_J,m_J}(t). \tag{16}$$

In the calculations, we assume that initially all Zeeman sublevels of the ground level are equally populated, without any coherences between them. The dependence of the Rabi frequency on magnetic quantum number m_J is given by the Clebsch-Gordon coefficients. Both laser fields are linearly polarized in the same direction, which also defines the quantization axis, to which the selection rule $\Delta m_J=0$ refers. The Rabi frequencies for each ladder of three m_J sublevels are obtained from the mean Rabi frequencies as

$$\Omega_P(m_J) = \frac{1.061}{8}\sqrt{8^2 - m_J^2}\Omega_P, \tag{17}$$

$$\Omega_S(m_J) = \frac{1}{9}\sqrt{9^2 - m_J^2}\Omega_S, \tag{18}$$

where $\Omega_P/2\pi=339$ MHz and $\Omega_S/2\pi=3$ MHz.

Next we perform convolution over magnetic sublevels and thermal velocity distributions. It is instructive to inspect the spectral profiles with only some of the averages executed.

1. Convolution of spectral profiles over m_J

The dotted lines in Fig. 5 show examples of the calculated excitation spectra of level f at a moderate P-laser detuning of

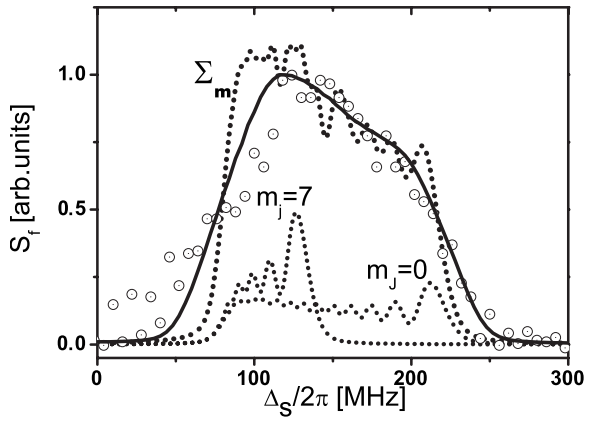

FIG. 5. Anatomy of excitation spectrum of level f as a function of S-laser detuning for a P-laser detuning $\Delta_P/2\pi=-80$ MHz and Rabi frequency $\Omega_P/2\pi=339$ MHz. The dotted lines are signals calculated for molecules traveling along the particle beam axis with the flow velocity v_m. The transit time across the P-laser beam is $\tau_{tr}\simeq 75$ ns. The electronic lifetimes are $\tau_e=12.45$ ns and $\tau_f=35$ ns. The lines labeled $m_J=0$ and $m_J=7$ are the partial excitation spectra for ladders with the given m_J quantum numbers, while Σ_m is the total signal related to the sum of all eight separate ladders with $0\leqslant m_J\leqslant 7$. Finally, the solid line is the total signal, which takes into account the finite width of the velocity distribution of molecules in the beam both parallel and perpendicular to the particle beam axis. The open circles (with a central dot) show experimental results [see Fig. 3(b)].

$\Delta_P/2\pi=-80$ MHz for the two g-e-f ladders (see Fig. 1) of three sublevels with either $m_J=0$ or $m_J=7$. The averaging of the velocity distributions is not yet executed. Ladder systems associated to other m_J (not shown) exhibit a similar structure, intermediate between the two limiting cases shown. The dashed-dotted line shows the profile resulting from summing all partial profiles with $m_J=0,\ldots,7$.

The coherences in the density matrix have relatively little influence on the result for our particular level system. This is because only 5% of the population returns from level e to level g by spontaneous emission to the ground level, while level f is only weakly populated. Trial calculations excluding Zeeman and optical coherences yielded excitation spectra that differ negligibly from those shown in Fig. 5.

2. Evidence for interference structure

The excitation spectra of a specific m_J state (see Fig. 5), shows an oscillatory structure, which results from the evolution along two interfering paths (see Fig. 4). The latter figure shows the variation of the eigenvalues ε_- and ε_+ across the P-laser beam profile, together with the energy ε_f of state f, which is weakly coupled by the S laser (see Fig. 1) to the Φ_- state.

A fraction of the population which evolves initially along the ε_- path is transferred to the ε_f path at the location where ε_- and ε_f cross. The Landau-Zener theory [15,16] could be used for a quantitative analysis of the branching of the population into the two paths at this crossing. Depending on the electronic lifetime (in comparison to the transit time through the laser beam) some of the population in the Φ_- state and the f state will decay to levels outside the considered level system. The amplitudes of the fraction of the population, which survives the evolution along the two paths, will be superimposed at the second crossing of ε_- and ε_f. Here the population either continues to evolve along the same path or transfers to the other one. Again, the Landau-Zener theory would allow a quantitative analysis. Whether the population which is asymptotically observed in state f is enhanced or reduced by interference, depends on the phase difference $\Delta_{\Phi_-,f}$ accumulated during the evolution along ε_- and ε_f between the two crossing points.

When the S-laser frequency is changed, the energy ε_f changes relative to the asymptotic value of ε_-. Accordingly, the area enclosed by ε_- and ε_f, as well as the distance between the two crossings, and thus the relative phase $\Delta_{\Phi_-,f}$ changes. An obvious consequence is the interference structure seen in Fig. 5 (dotted curves) for the excitation spectra related to $m_J=0$ and $m_J=7$. Since the Rabi frequency is larger for $m_J=0$ than for $m_J=7$, the structure for the former extends over a larger frequency range. When the S-laser detuning Δ_S is set to such a value that ε_f is tangential to the maximum of ε_-, the Landau-Zener theory predicts an enhanced transition rate. In fact, a global maximum is seen in the excitation spectra of Fig. 5 (dotted curves) for such value of the detuning Δ_S. For an even larger detuning of Δ_S, the curves ε_- and ε_f do not cross and the excitation probability vanishes, as confirmed by the spectra shown in Fig. 5. In Sec. VI we will consider the question under which conditions this interference structure can be resolved experimentally and also speculate about potentially interesting applications of these features.

An example of a similar interference structure, resulting from time-separated interactions during a single pulse, was reported in [17]. In that study, a three-state ladder system of sodium atoms interacted with two simultaneous laser pulses: a strong pulse, coupling the ground state g to the intermediate state e, together with a weak probe pulse coupling the intermediate level to the upper state f (see Fig. 1). The strong-pulse frequency was tuned to and kept on resonance with the g-e transition, while the frequency of the probe pulse was varied across the e-f resonance, revealing an AT doublet. The time-dependent AT splitting, determined by the time-dependent laser intensity, allowed resonant interaction induced by the probe field once during the rise, and again during the fall of the laser intensity. The interference of these two excitation pathways caused an oscillatory dependence of the f-level fluorescence on the frequency of the probe laser. The present study differs from the earlier work reported in [17] in several aspects. Our observations are not made by exposing a thermal ensemble of sodium atoms to short laser pulses, rather they are in a molecular beam. In our experiment the exposure of the molecules to the radiation fields is long compared to the radiative lifetime of levels e and f. Thus optical pumping becomes significant.

3. Convolution over velocity distributions

The finite width of the velocity distribution for the molecules in the beam has two consequences. The motion perpendicular to the particle beam axis, i.e., parallel to the laser

beams, leads to a distribution of Doppler shifts, while the motion parallel to the particle beam axis, i.e., perpendicular to the laser beam axis, leads to a distribution of transit times across the laser beams. The former can be modified by varying the collimation angle of the molecular beam, whereas the latter can be influenced only to a small extent by varying the temperature of the beam source or by adding a carrier gas such as He or Ar [18]. The profile resulting from the convolution over the sum of all partial profiles with $m_J=0,\ldots,7$, including the distribution of Doppler shifts and transit times in our experiment, is shown as a solid line in Fig. 5.

C. Conclusion

Figure 5 shows an example of how the complex line shape derives from the superposition of the spectral profile of individual m_J states. The solid lines in Fig. 3 show the fully averaged and convoluted numerical results for different detunings of the P laser. The excellent agreement with the experimental observations confirms the validity of the numerical procedure used here, which does not allow for any adjustable parameters. In fact, because of the emission characteristics of polarized light the observed fluorescence intensity does not precisely follow the magnetic sublevel populations. However, numerical test calculations showed that the alignment in the f level due to the laser excitation process and a small flow-induced prealignment of molecules in a supersonic beam [19] yields lineshapes that differ only slightly (by less than 5%, i.e., within the experimental error bars) in the shoulder seen in the right-hand side of Fig. 3.

VI. CONSEQUENCES OF INTERFERENCE

It is apparent from Fig. 5 that the summing of m_J sublevels strongly affects the oscillatory structure of the excitation spectrum (see Sec. V B), leaving but a few shallow oscillations. Further convolution with the Doppler shift and the distribution of transit times completely blurs the structure, leaving only a broad spectral profile, possibly with an indication of a shoulder. Although the Doppler broadening could be further reduced by tighter collimation of the molecular beam and by using counterpropagating P and S lasers, it is not possible to resolve the interference structure in the present experiment since we have only limited control over the distribution of transit times. Nevertheless, it is interesting to identify the condition which would allow seeing the signature of the interference.

We consider a three-state ladder such as the one shown in Fig. 1, except that the rotational levels are $J_g=1\leftrightarrow J_e=0\rightarrow J_f=1$, and electronic lifetime τ_f is chosen to be much larger than the transit time of the molecules through the laser beams. In this case we have no degeneracies, since with linearly polarized P and S lasers only the $m_J=0$ states in the g, e, and f levels are involved. Figure 6 shows some results, with the spatial distribution of the population in state f presented in the upper part, the adiabatic eigenvalues ε_- (thick solid line) and two choices of the eigenvalue ε_f (thin solid line) for different detunings of the S laser in the left lower frame, and the total population in the f level as a function of the detuning Δ_S in the right lower frame.

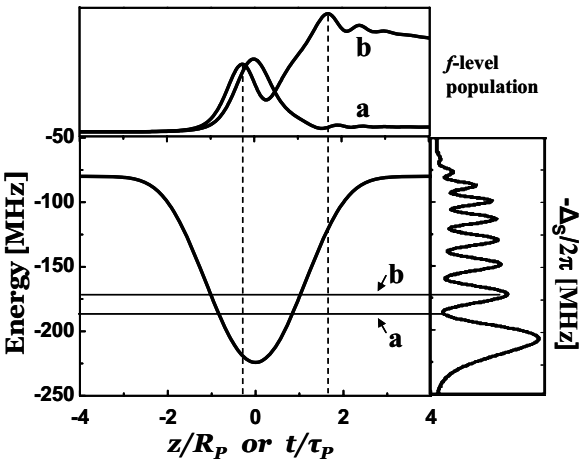

FIG. 6. Calculated spatial distributions of the population of level f as a function of the spatial coordinate z along the molecular beam axis for the ladder of Zeeman sublevels with $m_J=0$. The detuning of the P laser field is fixed at $\Delta_P/2\pi=80$ MHz. The plots show the spatial distributions calculated using a transit time $\tau_{tr}\simeq 37.5$ ns, and electronic lifetimes $\tau_e=12.45$ ns and $\tau_f=300$ ns. The lines **a** and **b** correspond to the S-laser frequency tuned to an interference minimum or maximum, respectively.

Let us consider the population of level f at a location downstream of the second crossing $P_f(\infty,\Delta_S,\Delta_{\Phi\_f})$, where Δ_{Φ_f} is the phase difference accumulated during propagation along the two paths. Since Δ_S controls the spatial region of the crossing of ε_- and ε_f, and thus controls the relative phase Δ_{Φ_f}, Δ_S may be tuned either to a maximum or to a minimum of the interference structure. Depending on the contrast ratio of the oscillation, a small detuning Δ_S may result in a substantial change of the f-level population.

Trace **a** (upper frame of Fig. 6) shows the spatial variation of the f-level population when Δ_S is tuned to a minimum of $P_f(\infty,\Delta_S,\Delta_{\Phi\_f})$, while trace **b** relates to Δ_S tuned to a maximum of $P_f(\infty,\Delta_S,\Delta_{\Phi\_f})$. In case **a** the f-level population is restricted to a relatively narrow region near the first crossing of eigenvalues, while in case **b** it extends over a much larger region. The enhancement of the population by constructive interference beyond the second crossing of the eigenvalues is clearly seen in the latter case. Beyond that crossing $P_f(\infty,\Delta_S,\Delta_{\Phi\_f})$ decays by spontaneous emission. The f-level population downstream of the first crossing is not only subject to spontaneous emission loss, but also to (partial) Rabi oscillation, which is seen as long as the S laser induces coupling between the e and the f level, i.e., at locations close to the point where the eigenvalues ε_- and ε_f cross.

Figure 7 shows the simulated excitation spectrum of level f for small, intermediate, and large Rabi frequency Ω_S prior to the convolution with the distribution of transit times. At very large Rabi frequencies (trace **3**) the contrast ratio of the oscillatory structure is very small, since the crossing of ε_- and ε_f is adiabatically avoided and most of the population evolves along only one of the two paths. At small Rabi frequencies, interference fringes are seen. In this range the contrast ratio is not sensitive to Δ_S for the following reason. The

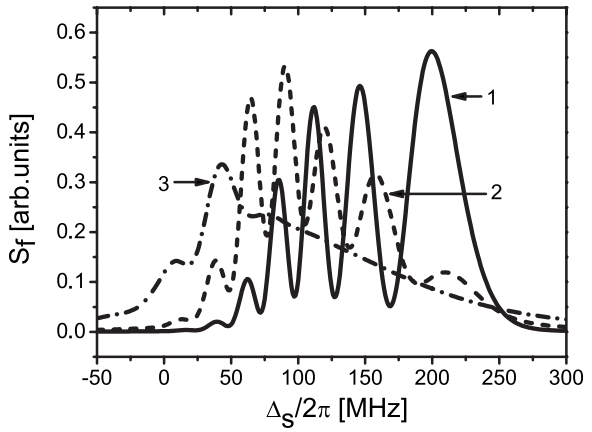

FIG. 7. Calculated excitation spectrum of level f as a function of S-laser detuning for various values of S-laser Rabi frequency Ω_S: trace 1—$\Omega_S/2\pi=35$ MHz; trace 2—$\Omega_S/2\pi=87$ MHz; trace 3—$\Omega_S/2\pi=173$ MHz. The P-laser detuning $\Delta_P/2\pi=-80$ MHz. The lifetime $\tau_f=100$ ns and transit time $\tau_{tr}=18.75$ ns. The other parameters (m_J, τ_e) are the same as for Fig. 6.

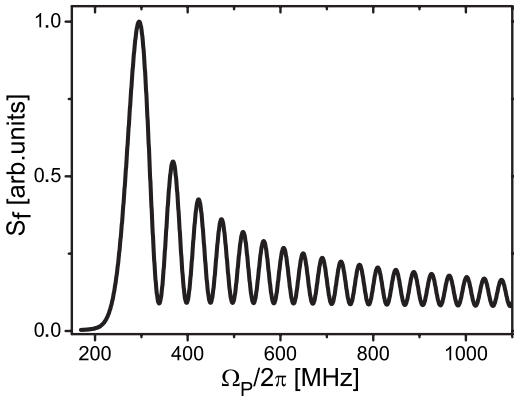

FIG. 8. Calculated excitation spectrum of level f as a function of P-laser Rabi frequency Ω_P. The laser detunings $\Delta_P/2\pi=-80$ MHz and $\Delta_S/2\pi=186$ MHz correspond to the first minimum of Fig. 6 for $\Omega_P/2\pi=339$ MHz. The lifetime $\tau_f=100$ ns and the other parameters $(m_J, \tau_{tr}$, and $\tau_e)$ are the same as for Fig. 6.

population is initially in state Φ_-. At the first crossing, a fraction $\eta(\Omega_S)\ll 1$ branches off and follows ε_f, while the fraction $(1-\eta)$ proceeds along Φ_-. At the second crossing, the fraction $(1-\eta)$, which has evolved along ε_f, will continue along ε_f beyond the crossing. Thus, the contribution of this path to $P_f(\infty, \Delta_S, \Delta_{\Phi_-,f})$ will be proportional to $\eta(1-\eta)$. Accordingly, a fraction η of the population, which has evolved along ε_- will branch off into ε_f. Thus, the contribution of this path to $P_f(\infty, \Delta_S, \Delta_{\Phi_-,f})$ will also be proportional to $\eta(1-\eta)$. Therefore, the relative amplitude of the two interfering amplitudes does not change and thus, the contrast ratio is not sensitive to Δ_S.

The outcome of the interference is sensitive to the P-laser Rabi frequency because the area enclosed between the two transfer paths depends on that. This is illustrated by numerical results shown in Fig. 8 for fixed S- and P-laser detunings. The population $P_f(\infty, \Delta_S, \Delta_{\Phi_-,f})$ oscillates with Ω_P, while the decreased contrast for larger Ω_P is due to population loss via optical pumping. Figure 8 also shows the requirement regarding the stability of the P-laser intensity: the tolerable fluctuations of Ω_P are on the level of 10%, which can be easily achieved in the experiment.

VII. SUMMARY AND OUTLOOK

We have demonstrated that population loss from an open molecular three-level system g-e-f, with levels g and e coupled by a strong laser field P and levels e and f coupled by a weak field S, suppresses the appearance of an Autler-Townes doublet in the excitation spectrum of level f. Instead, a spectral structure is observed, which is relatively narrow when the P laser is on resonance, but broadens at moderate detuning with its center shifted in frequency, before narrowing again at large P-laser frequency detuning. We have also shown that interference due to two spatially separated crossings with an adiabatic state does occur but is not resolved in the present experiment due to convolution of the excitation spectrum over initial population distribution in magnetic sublevels of the ground level. The distribution of Doppler shifts results from a finite collimation angle, and the distribution of transit times of molecules through the laser beams is due to thermal velocity distribution. The resolution can be improved by using excitation geometries that exclude the Doppler broadening.

When the lifetime of state f is long compared to the transit time, the population will reach level f at the first crossing of ε_- and ε_f. The population will only marginally change until the second crossing is reached. Control of the detuning may lead to a sudden decrease of the f-level population beyond this crossing or to an enhancement.

We also note in passing that the same type of reasoning would be valid for the excitation of atoms in an ultracold gas to an, e.g., Rydberg state. Since ultracold atoms are stationary on the time scale relevant here, the f-level population is controllable as a function of time, rather than space.

ACKNOWLEDGMENTS

This work was supported by the EU-FP6-TOK project LAMOL (Contract No. MTKD-CT-2004-014228), NATO Grant No. EAP.RIG.981378, Latvian Science Council, and European Social Fund. The authors thank B. W. Shore for the very helpful discussions and comments on the earlier version of the manuscript, and C. Andreeva for editorial assistance.

[1] C. Delsart and J. C. Keller, J. Phys. B **9**, 2769 (1976); J. L. Picque and J. Pinard, *ibid.* **9**, L77 (1976); H. R. Gray and C. R. Stroud Jr., Opt. Commun. **25**, 359 (1978).

[2] (This is a selection out of several hundreds of papers published.) A. M. Bonch-Bruevich, N. N. Kostin, V. A. Khodovoi, and V. V. Khromov, Sov. Phys. JETP **29**, 82 (1969); P. T. H. Fisk, H. A. Bachor, and R. J. Sandeman, Phys. Rev. A **33**, 2418 (1986); **33**, 2424 (1986); **34**, 4762 (1986); B. K. Teo, D. Feldbaum, T. Cubel, J. R. Guest, P. R. Berman, and G. Raithel, *ibid.* **68**, 053407 (2003); J. A. Beswick, C. R. Seances Acad. Sci., Ser. B **270**, 245 (1970); C. Cohen-Tannoudji and S. Reynaud, J. Phys. B **10**, 345 (1977); W. A. McClean and S. Swain, *ibid.* **10**, L143 (1977); R. M. Whitley and C. R. Stroud, Jr., Phys. Rev. A **14**, 1498 (1976); J. P. D. Martin, *ibid.* **57**, 2002 (1998); M. Bosticky, Z. Ficek and B. J. Dalton, *ibid.* **57**, 3869 (1998); F. C. Spano, J. Chem. Phys. **114**, 276 (2001).

[3] B. Girard, G. O. Sitz, R. N. Zare, N. Billy, and J. Vigue, J. Chem. Phys. **97**, 26 (1992); A. F. Linskens, N. Dam, J. Reuss, and B. Sartakov, *ibid.* **101**, 9384 (1994); J. Qi, G. Lazarov, X. Wang, L. Li, L. M. Narducci, A. M. Lyyra, and F. C. Spano, Phys. Rev. Lett. **83**, 288 (1999); P. Yi, M. Song, Y. Liu, R. W. Field, L. Li, and A. M. Lyyra, Opt. Commun. **233**, 131 (2004).

[4] R. Garcia-Fernandez, A. Ekers, J. Klavins, L. P. Yatsenko, N. N. Bezuglov, B. W. Shore, and K. Bergmann, Phys. Rev. A **71**, 023401 (2005).

[5] S. H. Autler and C. H. Townes, Phys. Rev. **100**, 703 (1955).

[6] G. Baumgartner, H. Kornmeier, and W. Preuss, Chem. Phys. Lett. **107**, 13 (1984).

[7] A. Ekers, T. Kirova, K. Miculis, K. Blushs, M. Auzinsh, N. N. Bezuglov, R. Garcia-Fernandez, K. Bergmann, L. P. Yatsenko, O. Dulieu, and M. Aymar, *Determination of Lifetimes of Excited Molecular States using the Autler-Townes Effect*, in Abstracts of the 20th International Conference on Atomic Physics (ICAP XX), edited by Ch. Roos and H. Häffner (Innsbruck, Austria, 2006), p. 108.

[8] H. R. Gray and C. R. Stroud, Opt. Commun. **25**, 359 (1978).

[9] J. L. Picqé and J. Pinard, J. Phys. B **9**, L77 (1976).

[10] B. W. Shore, *The Theory of Coherent Atomic Excitation* (Wiley, New York, 1990).

[11] M. Auzinsh and R. Ferber, *Optical Polarization of Molecules* (Cambridge University Press, Cambridge, 1995).

[12] C. Cohen-Tannoudji, J. Dupont-Roc, and G. Grynberg, *Atomo-Photon Interactions* (Wiley, New York, 1992).

[13] M. D. Fiet, J. A. Fleck, and A. Steiger, J. Comput. Phys. **47**, 412 (1982).

[14] A. K. Kazansky, N. N. Bezuglov, A. F. Molisch, F. Fuso, and M. Allegrini, Phys. Rev. A **64**, 022719 (2001).

[15] L. D. Landau, Phys. Z. Sowjetunion **2**, 46 (1932); C. Zener, Proc. R. Soc. London, Ser. A **137**, 696 (1932).

[16] E. E. Nikitin, *Theory of Elementary Atomic and Molecular Processes in Gases* (Clarendon Press, Oxford, 1974).

[17] S. R. Wilkinson, A. V. Smith, M. O. Scully, and E. Fry, Phys. Rev. A **53**, 126 (1996).

[18] H. Pauly, in *Atomic and Molecular Beam Techniques*, edited by G. Scoles (Oxford University Press, New York, 1988), Vol. 1, p. 124.

[19] U. Hefter, G. Ziegler, A. Mattheus, A. Fischer, and K. Bergmann, J. Chem. Phys. **85**, 286 (1986).

[20] Note, that ε_- and ε_+ are adiabatic states for the Hamiltonian H given by Eq. (3), while ε_-, ε_+, and ε_f are diabatic states for the Hamiltonian H' given by Eq. (12).